


## Possible coexistence of superconductivity and topological electronic states in 1T-RhSeTe

Tengdong Zhang(张腾东), Rui Fan(樊睿), Yan Gao(高炎), Yanling Wu(吴艳玲), Xiaodan Xu(徐晓丹), Dao-Xin Yao(姚道新), and Jun Li(李军)

**Citation:**Chin. Phys. B, 2025, 34 (**2**): 027403. DOI: 10.1088/1674-1056/ada432
Journal homepage: http://cpb.iphy.ac.cn; http://iopscience.iop.org/cpb

**What follows is a list of articles you may be interested in**

---

## Phonon-mediated superconductivity in orthorhombic *X*S (*X* = Nb, Ta or W)

Guo-Hua Liu(刘国华), Kai-Yue Jiang(江恺悦), Yi Wan(万一), Shu-Xiang Qiao(乔树祥), Jin-Han Tan(谭锦函), Na Jiao(焦娜), Ping Zhang(张平), and Hong-Yan Lu(路洪艳)
Chin. Phys. B, 2025, 34 (**2**): 027401. DOI: 10.1088/1674-1056/ad9733

## Intermediately coupled type-II superconductivity in a La-based kagome metal $La_3Al$

Yingpeng Yu(于英鹏), Zhaolong Liu(刘兆龙), Zhaoxu Chen(陈昭旭), Qi Li(李琦), Yulong Wang(王玉龙), Xuhui Wang(王旭辉), Chunsheng Gong(龚春生), Zhaotong Zhuang(庄照通), Bin-Bin Ruan(阮彬彬), Huifen Ren(任会芬), Peijie Sun(孙培杰), Jian-Gang Guo(郭建刚), and Shifeng Jin(金士锋)
Chin. Phys. B, 2025, 34 (**1**): 017401. DOI: 10.1088/1674-1056/ad8f9f

## Half-integer Shapiro steps in $MgB_2$ focused He ion beam Josephson junctions

Dali Yin(殷大利), Xinwei Cai(蔡欣炜), Tiequan Xu(徐铁权), Ruining Sun(孙瑞宁), Ying Han(韩颖), Yan Zhang(张焱), Yue Wang(王越), and Zizhao Gan(甘子钊)
Chin. Phys. B, 2024, 33 (**8**): 087404. DOI: 10.1088/1674-1056/ad4d62

## Two-fold symmetry of the in-plane resistance in kagome superconductor

## $Cs(V_{1-x}Ta_x)_3Sb_5$ with enhanced superconductivity

Zhen Zhao(赵振), Ruwen Wang(王汝文), Yuhang Zhang(张宇航), Ke Zhu(祝轲), Weiqi Yu(余维琪), Yechao Han(韩烨超), Jiali Liu(刘家利), Guojing Hu(胡国静), Hui Guo(郭辉), Xiao Lin(林晓), Xiaoli Dong(董晓莉), Hui Chen(陈辉), Haitao Yang(杨海涛), and Hong-Jun Gao(高鸿钧)
Chin. Phys. B, 2024, 33 (**7**): 077406. DOI: 10.1088/1674-1056/ad4ffa

## Observation of parabolic electron bands on superconductor $LaRu_2As_2$

Xingtai Zhou(周兴泰), Geng Li(李更), Lulu Pan(潘禄禄), Zichao Chen(陈子超), Meng Li(李萌), Yanhao Shi(时延昊), Haitao Yang(杨海涛), and Hong-Jun Gao(高鸿钧)
Chin. Phys. B, 2024, 33 (**7**): 077401. DOI: 10.1088/1674-1056/ad4d63

---

**RAPID COMMUNICATION**

# Possible coexistence of superconductivity and topological electronic states in 1T-RhSeTe

Tengdong Zhang(张腾东)[1,†], Rui Fan(樊睿)[1,†], Yan Gao(高炎)[1], Yanling Wu(吴艳玲)[1], Xiaodan Xu(徐晓丹)[1], Dao-Xin Yao(姚道新)[2,‡], and Jun Li(李军)[1,§]

[1] *Hebei Key Laboratory of Microstructural Material Physics, School of Science, Yanshan University, Qinhuangdao* 066004, *China*
[2] *State Key Laboratory of Optoelectronic Materials and Technologies, Guangdong Provincial Key Laboratory of Magnetoelectric Physics and Devices, School of Physics, Sun Yat-Sen University, Guangzhou* 510275, *China*

(Received 14 October 2024; revised manuscript received 26 December 2024; accepted manuscript online 31 December 2024)

Transition metal dichalcogenides (TMDs), exhibit a range of crystal structures and topological quantum states. The 1T phase, in particular, shows promise for superconductivity driven by electron–phonon coupling (EPC), strain, pressure, and chemical doping. In this theoretical investigation, we explore 1T-RhSeTe as a novel type of TMD superconductor with topological electronic states. The optimal doping structure and atomic arrangement of 1T-RhSeTe are constructed. Phonon spectrum calculations validate the integrity of the constructed doping structure. The analysis of the electron–phonon coupling using the electron–phonon Wannier (EPW) method has confirmed the existence of a robust electron–phonon interaction in 1T-RhSeTe, resulting in total EPC constant $\lambda = 2.02$, the logarithmic average frequency $\omega_{\log} = 3.15$ meV and $T_c = 4.61$ K, consistent with experimental measurements and indicative of its classification as a BCS superconductor. The band structure analysis revealed the presence of Dirac-like band crossing points. The topological non-trivial electronic structures of the 1T-RhSeTe are confirmed via the evolution of Wannier charge centers (WCCs) and time-reversal symmetry-protected topological surface states (TSSs). These distinctive properties underscore 1T-RhSeTe as a possible candidate for a topological superconductor, warranting further investigation into its potential implications and applications.

**Keywords:** superconductivity, topological electronic state, transition metal dichalcogenides

**PACS:** 74.70.–b, 63.20.kd, 73.20.At, 74.62.Dh, 71.15.Mb

**DOI:** 10.1088/1674-1056/ada432 **CSTR:** 32038.14.CPB.ada432

## 1. Introduction

Transition metal dichalcogenides (TMDs) are compounds represented by the chemical formula $MX_2$, where $M$ denotes transition metals such as Mo, W, and Ni, and $X$ represents chalcogen elements such as S, Se, and Te. Featuring a layered structure, TMDs display a remarkable degree of diversity and exhibit a variety of topological quantum states, including Weyl semimetal, topological insulator, and quantum spin Hall effect.[1–3] TMDs can adopt various crystal structures, with the most prevalent being hexagonal (2-H), rhombohedral (3-R), and trigonal (1-T) phases. The 2-H phase typically manifests as a semiconductor and is the most thermodynamically stable, while the 1-T phase exhibits metallic behavior and possesses distinctive topological properties.[4–6]

The superconducting behaviors of 1-T phase TMDs are intrinsic or induced by chemical doping or applied strain.[7–9] For example, both 1T-$TiSe_2$ and 1T-$PdTe_2$ exhibit semimetallic characteristics, and the topological superconductivity can be driven by electron–phonon coupling (EPC). Experimental observations have revealed that 1T-$TiSe_2$ exhibits a superconducting transition temperature ($T_c$) of 2 K under a pressure of 3 GPa, while the $T_c$ of $PdTe_2$ is 1.7 K.[10,11] In the 1-T phases of $PtTe_2$, $PdSe_2$, $NiTe_2$, and $PdTe_2$, the Dirac cone is tilted, and forms a type-II Dirac topological point.[12–15] Furthermore, the Dirac point in $NiTe_2$ is situated at the Fermi energy level of 0.80 meV, and the position of the Fermi energy can be adjusted through strain, pressure, and chemical doping.[9] 1T-phase TMDs hold significant promise for inducing superconductivity with topological quantum states.

Generally, a superconductor is regarded as topological if any of the topological numbers is nonzero.[16,17] Topological superconductors have emerged as a fascinating area of research in quantum computing due to their unique physical properties and potential applications.[18–20] They offer an ideal platform for studying fundamental quantum physics problems, such as non-Abelian anyons and quantum entanglement, and propose possible solutions for building future quantum computers that can achieve fault-tolerant quantum computation.[18,19,21] Topological superconductors are closely associated with Majorana fermions, which are exotic particles that are their own antiparticles.[19,22]

A novel Dirac semimetal, 1T-RhSeTe, has been identi-

[†]These authors contributed equally to this work.
[‡]Corresponding author. E-mail: yaodaox@mail.sysu.edu.cn
[§]Corresponding author. E-mail: ljcj007@ysu.edu.cn

© 2025 Chinese Physical Society and IOP Publishing Ltd. All rights, including for text and data mining, AI training, and similar technologies, are reserved.

fied as a superconductor with $T_c = 4.72$ K.[23] In 1T-RhSeTe, selenium (Se) replaces tellurium (Te) atoms in the 1T phase of $RhTe_2$, a TMD previously reported to lack superconductivity and topological electronic states.[24,25] This substitution induces superconductivity and topological electronic states, which is a possible candidate for topological superconductors.

This study employs density-functional theory (DFT) within first-principles calculations to examine the electronic bands, phonon, superconductivity, and topological characteristics of 1T-RhSeTe. Analysis of the electron–phonon coupling and Eliashberg spectral function yields the EPC strength ($\lambda = 2.02$) and $T_c = 4.61$ K.

Furthermore, a Dirac cone crosses near the Fermi energy in the absence of spin–orbit coupling (SOC). However, the presence of the SOC effect results in the Dirac cone becoming gapped, thereby manifesting a Dirac-type surface state that is protected by time-reversal symmetry. The calculated $\mathbb{Z}_2$ topological index is $\mathbb{Z}_2 = 1$, indicating that 1T-RhSeTe is in a strongly topological electronic state.

## 2. Computational details

We use the projector-augmented wave method implemented in the Vienna *Ab initio* Simulation Package (VASP) to perform DFT calculations for the structure optimization.[26] The generalized gradient approximation (GGA) and the Perdew–Burke–Ernzerhof (PBE) function are used to treat the electron exchange–correlation potential.[27,28] In the computation, the plane wave cut-off energy is set at 700 eV, a Monkhorst–Pack $k$ lattice with a spacing of $2\pi \times 0.03$ Å$^{-1}$ is employed, and the structure is optimized using optB88-vdW van der Waals (vdW) interaction corrections[29] until the force on each atom is less than 0.015 eV × Å$^{-1}$.

Quantum Espresso (QE) is used for DFT calculations including self-consistent, band structure, and phonon calculations.[30] The PBE generalization of GGA is the basis for the exchange–correlation generalization. The calculations use kinetic energy cutoff values of 70 Ry for the wave function and 700 Ry for the potential function, a $6\times6\times6$ $k$-grid, and a $6\times6\times6$ $q$-point grid. The self-consistent convergence threshold is set to $1\times10^{-10}$ Ry. The d-orbitals of the Rh atoms, the p-orbitals of the Te atoms, and the p-orbitals of the Se atoms are selected as the projected orbits, and the $6\times6\times6$ $k$-mesh grid is set up to construct the tight-binding Hamiltonian for the established structure by the software package wannier90 based on maximally localized Wannier functions (MLWFs).[31,32]

The electron–phonon Wannier (EPW) code[33] is employed to obtain the electron–phonon coupling and BCS superconductivity. The $k$-mesh and $q$-mesh grids are uniformly increased to $20\times20\times20$ for more accurate results. The EPW code solves the Eliashberg equation and related superconductivity equations to calculate electron–phonon coupling strength and $T_c$. The electron–phonon coupling constant $\lambda$ can be calculated by

$$\lambda = 2\int \frac{\alpha^2(\omega)}{\omega}\,\mathrm{d}\omega, \tag{1}$$

where $\alpha^2F(\Omega)$ is the Eliashberg spectral function, the phonon density of states weighted by an electron–phonon coupling matrix element at each $k$-point and frequency. The superconducting $T_c$ is determined with the McMillan equation modified by Allen–Dynes formula[34,35]

$$T_c = \frac{f_1 f_2 \omega_{\log}}{1.2}\exp\left[\frac{-1.04(1+\lambda)}{\lambda(1-0.62\mu^*)-\mu^*}\right], \tag{2}$$

where $\mu^*$ is the effective screened Coulomb repulsion constant typically ranging from 0.1 eV to 0.16 eV, and the logarithmically averaged frequency $\omega_{\log}$ can be defined as

$$\omega_{\log} = \exp\left[\frac{2}{\lambda}\int\frac{\mathrm{d}\omega}{\omega}\alpha^2F(\omega)\ln\omega\right]. \tag{3}$$

We use WannierTools[36] to get WCCs[37] to reflect the topological properties of time-reversal invariant systems. $\mathbb{Z}_2$ topological invariant[38,39] is given by the number of times $L$ any line crosses a WCCs line when going from $k_i = 0$ to $k_i = \pi$

$$\mathbb{Z}_2 = L \mod 2. \tag{4}$$

The topological properties of three-dimensional materials can be classified using the $\mathbb{Z}_2$ topological index, classified by a set of indices $(\nu;\ \nu_x\,\nu_y\,\nu_z)$ defined through the 2D invariants on the time-reversal invariant planes in the Brillouin zone

$$\nu = \mathbb{Z}_2(k_i = 0) + \mathbb{Z}_2(k_i = 0.5) \mod 2, \tag{5}$$

$$\nu_i = \mathbb{Z}_2(k_i = 0.5), \tag{6}$$

where $k_i$ is in reduced coordinates. A system is referred to as a strong topological electronic state if $\nu = 1$.

## 3. Results and discussion

The 1T-RhSeTe sample obtained in the experiment was prepared by doping Te with Se, with an exact stoichiometry of $Rh_{1.01}Se_{1.05}Te_{0.94}$. Two potential doping structures, designated as type-I and type-II, are illustrated in Figs. 1(a) and 1(b), respectively. In the type-I doping of 1T-RhSeTe, Te atoms are substituted by Se atoms in a linear configuration, resulting in a zigzag arrangement of Te and Se atoms. This arrangement disrupts the inherent triple rotational symmetry of 1T-$RhTe_2$ and leads to a slightly shorter Se–Rh bond compared to the Te–Rh bond, thereby reducing the symmetry to $P2_1/m$ (No. 11). In contrast, the type-II doping of 1T-RhSeTe involves the replacement of Te atoms by Se atoms within a plane, where Te and Se atoms are distributed in planes, disrupting only the pre-existing $-3$ symmetry and reducing the symmetry to $P3m1$ (No. 156). The symmetry of type-I doping 1T-RhSeTe, which is $P2_1/m$ (No. 11), is lower than that

of type-II doping 1T-RhSeTe [$P3m1$ (No. 156)]. Both of these symmetries are lower than the $P$-$3m1$ (No. 164) symmetry of 1T-$RhTe_2$.

The lattice constants of the two structures following structural relaxation are presented in Table 1. Type-II doping of 1T-RhSeTe occupies a larger portion of the lattice within the plane, and the two different lengths of Se–Rh and Te–Rh bonds are forced to twist onto the same plane, resulting in a higher energy state compared to type-I doping 1T-RhSeTe. Significantly, the lattice constants of type-I doping 1T-RhSeTe are more closely aligned with experimental measurements, suggesting that the experimental measured 1T-RhSeTe is more likely to conform to type-I doping. Consequently, we only consider the type-I doping structure of 1T-RhSeTe in the subsequent analysis.

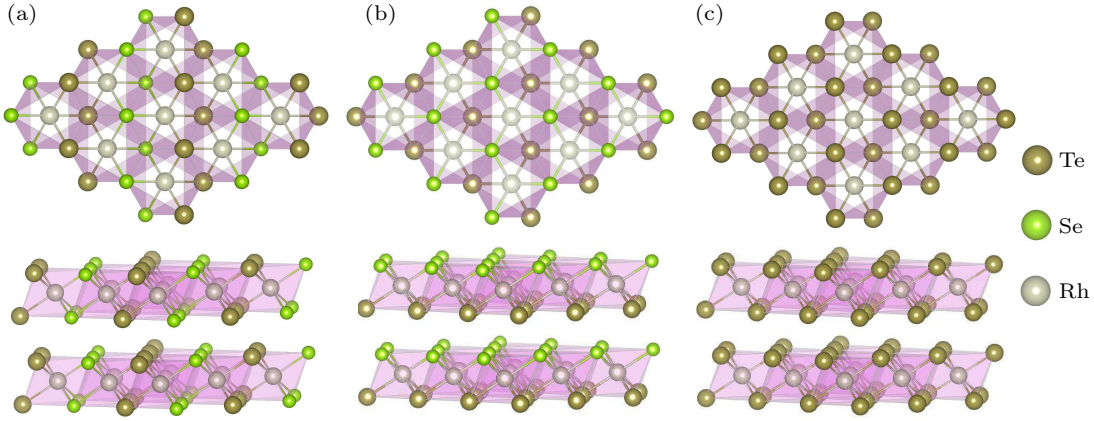



**Fig. 1.** Top and side views of the crystal structures of 1T-RhSeTe and $RhTe_2$: (a) type-I doping 1T-RhSeTe, where Se replaces Te atoms along lines; (b) type-II doping 1T-RhSeTe, where Se replaces Te atoms within plane; (c) 1T-$RhTe_2$.

**Table 1.** Lattice constants for type-I, type-II 1T-RhSeTe, compare with experiment and 1T-$RhTe_2$.

| Structure | Lattice constants (Å) | Energy (eV) | Ref. |
|---|---|---|---|
| Type-I | $a,b=3.794$, $c=5.363$ | −32.036 | calculation |
| Type-II | $a,b=3.818$, $c=5.291$ | −32.012 | calculation |
| Exper. | $a,b=3.798$, $c=5.389$ | | [23] |
| $RhTe_2$ | $a,b=3.938$, $c=5.513$ | | [24] |

Phonon dispersion represents a fundamental approach to assessing the dynamic stability of a system. The calculated phonon dispersions of 1T-RhSeTe are presented in Fig. 2. The absence of imaginary phonon modes in 1T-RhSeTe is indicative of its dynamic stability. The phonon dispersion can be classified into two distinct regions based on the vibration frequency. In the high-frequency region ($\omega \geq 110$ cm$^{-1}$), the majority of the phonons are composed of the vibration modes of Se and Te atoms. The Se atoms, which have the lowest mass, contribute the most to the higher-frequency phonons. The Te atoms engage in a seesaw-like resonance around the neighboring Rh atoms with Se atoms, thereby contributing to an additional portion of high-frequency phonons. In the low-frequency region, the phonons are formed by a combination of the vibrational modes of Rh and Te atoms, as these atoms are heavier and more localized in frequency space than Se atoms.

The calculated Eliashberg spectral function and integrated EPC strength are plotted in the right panel of Fig. 2. The distribution of the Eliashberg spectral function, $\alpha^2F(\Omega)$, in the high-frequency region is almost the same as in the low-frequency region. Notably, the vibration frequencies of the heavier elements, including Rh, Se, and Te, predominantly fall within the low-frequency range of 0–200 cm$^{-1}$. This behavior indicates findings from electron–phonon coupling calculations in heavier element superconductors, such as $LaBi_3$ and $LaCuSb_2$, where electron–phonon interactions are concentrated in the lower vibration frequency range.[40,41]

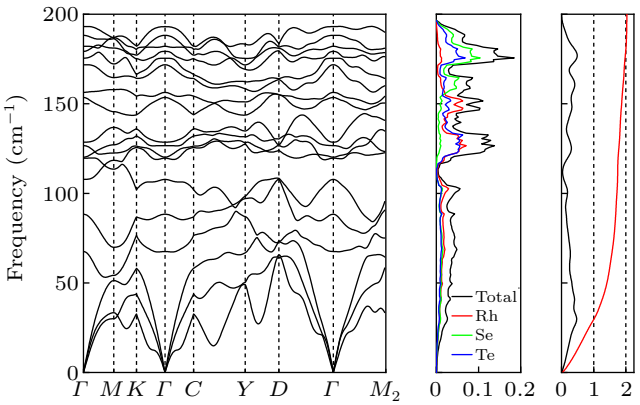



**Fig. 2.** The phonon spectrum of the type-I doping 1T-RhSeTe, phonon density of states (PHDOS), and Eliashberg spectral function $\alpha^2F(\omega)$.

The electron–phonon coupling in the low-frequency region peaks at around $\omega \sim 25$ cm$^{-1}$, with obvious in-plane vibration modes around the $M$–$K$ line. As indicated by Eq. (1), these in-plane vibration modes can result in a more pronounced EPC effect, thereby enhancing superconductivity. Around $\omega \sim 180$ cm$^{-1}$ in the high-frequency region, there is another EPC peak, which is mainly dominated by the seesaw-like vibration modes of Se and Te atoms.

Utilizing MLWFs, we derive the isotropic Eliashberg spectral function $\alpha^2F(\omega)$ for 1T-RhSeTe. The integration of $\alpha^2F(\omega)$ yields the total EPC constant $\lambda = 2.02$ and the logarithmic average frequency $\omega_{\log} = 3.15$ meV, indicating a strong electron–phonon coupling in the material. $T_c$ is estimated using the modified McMillan equation by Allen and Dynes. We select $\mu^* = 0.16$ eV considering the heavy elements Rh, Se, and Te. Consequently, we obtain $T_c = 4.61$ K, which is remarkably close to the experimental value of 4.72 K.[23] This calculation provides an evidence to the system's classification as a BCS superconductor, confirming the validity of our methods.

The energy band structure of 1T-RhSeTe is determined using QE, with and without SOC, as illustrated in Fig. 3. In the absence of SOC, the four energy bands closest to the Fermi level are distinctly separated from the remaining bands, exhibiting clear differentiation. It is noteworthy that the two energy bands in closest proximity to the Fermi level exhibit a band crossing along the $D$–$\Gamma$ direction. This crossing point is located very close to the Fermi level ($-0.01$ eV) and exhibits a linear dispersion, resulting in the formation of Dirac fermions that are analogous to those observed in graphene. The Fermi velocity at this point is $v_F = 1.71 \times 10^5$ m·s$^{-1}$, which is much lower than that of graphene ($\sim \times 10^6$ m·s$^{-1}$). This reduction in Fermi velocity can be attributed to the fact that these two bands are primarily derived from the p orbitals of Te. Given that the atomic mass of Te is significantly greater than that of C, the effective Fermi velocity is consequently much smaller than that observed in graphene.

A peak in the density of states (DOS) is observed at approximately 0.1 eV below the Fermi level, predominantly contributed by the Te atoms. This van Hove singularity in the electron band, associated with the Te atoms, is beneficial for the formation of superconductivity. Additionally, it is noteworthy that this van Hove singularity originates from a flat band along the $\Gamma$–$M$ direction. In conjunction with the aforementioned analysis of the low-frequency phonons contributed by Te atoms, it is proposed that this in-plane $\Gamma$–$M$ flat band is pivotal for the emergence of superconductivity. Building upon the previous findings on cuprate superconductors, we propose that electron doping or applying pressure could significantly enhance the superconductivity of 1T-RhSeTe, potentially approaching the McMillan limit.

In consideration of the SOC effect, the calculated band structure and DOS for 1T-RhSeTe are presented in Fig. 3(b). In comparison to the band structures without the SOC effect, the band structures undergo significant changes due to the pronounced SOC resulting from the large atomic mass. Each energy band splits into two bands when including SOC, demonstrating that the 1T-RhSeTe system adheres to time-reversal symmetry. The energy and momentum positions of the Dirac cone in the $\Gamma$–$D$ line are roughly 151 meV (another suspected Dirac cone at 115 meV) above the Fermi energy level. The calculation results indicate the presence of topological non-trivial states in 1T-RhSeTe.

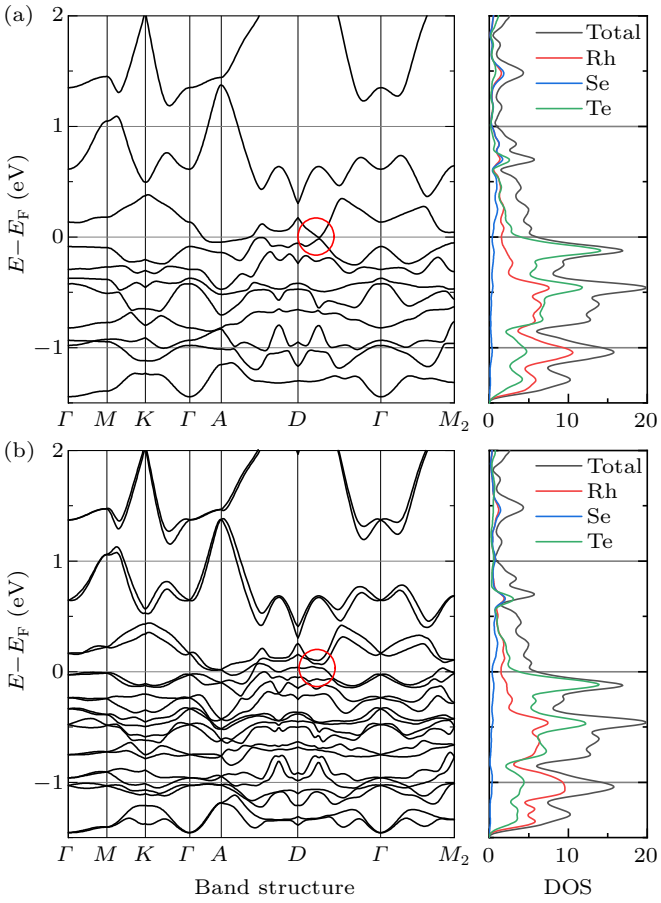



**Fig. 3.** Band structure and density of states of the type-I doping 1T-RhSeTe (a) without SOC and (b) including SOC obtained from DFT calculations. There is a Dirac point between $D$ and $\Gamma$ without SOC.

Figure 4 illustrates the evolution of WCCs in the six planes of the Brillouin zone. Three planes exhibit a topologically nontrivial state, leading to the determination of the topological $\mathbb{Z}_2$ index for 1T-RhSeTe represented as (1 ; 0 0 1). The first $\mathbb{Z}_2$ index is the strong index, while the last three $\mathbb{Z}_2$ numbers are the weak indices. This topological $\mathbb{Z}_2$ index indicates that 1T-RhSeTe has a strongly topological electronic state.

The plane formed by the high-symmetry points $D$, $\Gamma$, and $M$ is selected as the projection plane along the $K$–$\Gamma$–$M$–$K$ direction to depict the TSSs 1T-RhSeTe, as illustrated in Fig. 5. It can be observed that the time-reversal symmetry-protected TSSs emerge above the Fermi level by 0.151 eV at the $M$-point. Additionally, a potential TSS is detected 0.115 eV above the Fermi level at the $M$-point. These findings corroborate our earlier analysis regarding the robust topological electronic states in 1T-RhSeTe. The Se atoms doping can change the position of the Fermi energy level by replacing Te in 1T-$RhTe_2$ and then induce topological electronic states.

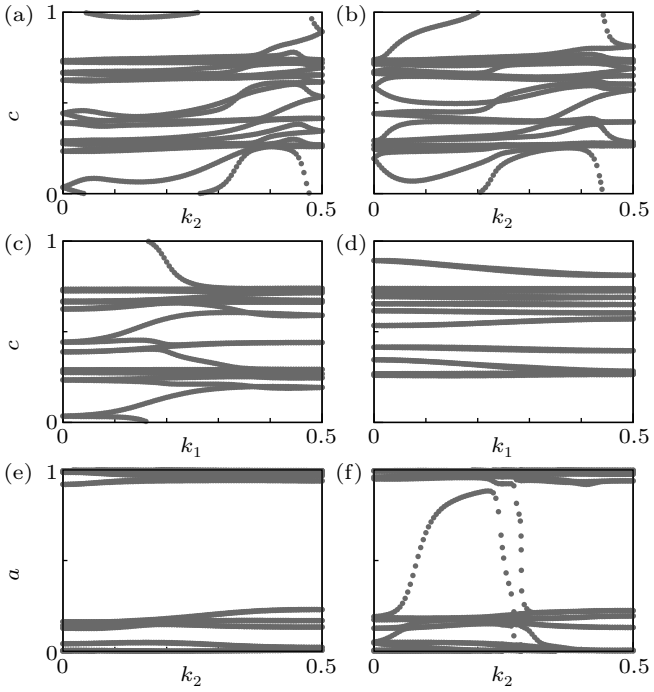



**Fig. 4.** The evolution of WCCs in the six planes of Brillouin zone. The $\mathbb{Z}_2$ invariants are (a) $k_1 = 0.0$, $k_2$–$k_3$ plane: $\mathbb{Z}_2 = 1$; (b) $k_1 = 0.5$, $k_2$–$k_3$ plane: $\mathbb{Z}_2 = 0$; (c) $k_2 = 0.0$, $k_1$–$k_3$ plane: $\mathbb{Z}_2 = 1$; (d) $k_2 = 0.5$, $k_1$–$k_3$ plane: $\mathbb{Z}_2 = 0$; (e) $k_3 = 0.0$, $k_1$–$k_2$ plane: $\mathbb{Z}_2 = 0$; (f) $k_3 = 0.5$, $k_1$–$k_2$ plane: $\mathbb{Z}_2 = 1$.

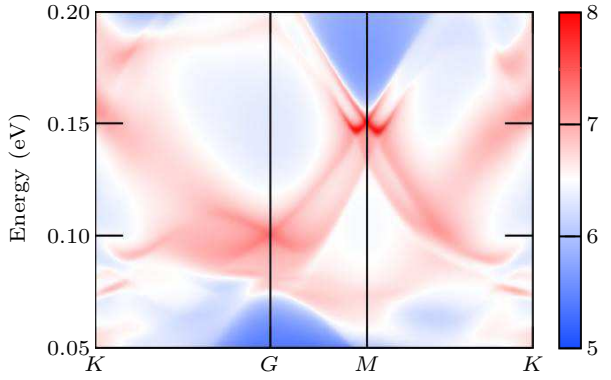



**Fig. 5.** TSSs of the 1T-RhSeTe on the (1 −1 2) surface along the *K*–*Γ*–*M*–*K* direction.

While the coexistence of nontrivial topological electronic states and superconductivity does not necessarily result in topological superconductivity in the bulk, it can induce topological superconductivity at the surface. The opening of a full gap, accompanied by a nontrivial $\mathbb{Z}_2$ index under SOC, gives rise to topologically nontrivial surface states. Due to its inherent two-dimensional characteristics, the bulk superconductivity can proximate to the surface, and when combined with the topologically nontrivial electronic structure of the surface, it can lead to helical topological superconductivity.[42–44]

There is potential to enhance both the topological and superconducting properties of 1T-RhSeTe. With regard to superconductivity, it can be posited that electron doping or the application of pressure could significantly enhance the superconducting properties of 1T-RhSeTe, given that the van Hove singularity and flat band in this material are in close proximity to the Fermi level. Our calculations indicate that introducing n-type doping, which lowers the Fermi level, results in a slight enhancement of the superconducting properties. However, this doping also causes the Dirac point to move further away from the Fermi level, leading to a loss of topological characteristics. On the other hand, applying pressure slightly reduces the superconducting properties. Therefore, careful tuning of this material could potentially yield better coexistence of topological and superconducting phases.[45]

## 4. Conclusion

In conclusion, theoretical calculations have been conducted on 1T-RhSeTe, which has been identified as a superconductor exhibiting topological electronic states. A doping structure and atomic arrangement for 1T-RhSeTe are constructed that optimize the material's properties. The integrity of the constructed doping structure is validated through phonon calculations. The analysis of the electron–phonon coupling using the EPW method confirms the existence of a robust electron–phonon interaction in 1T-RhSeTe. This has led to the determination of total EPC constant $\lambda = 2.02$, the logarithmic average frequency $\omega_{\log} = 3.15$ meV and $T_c = 4.61$ K, consistent with experimental measurements and indicative of its classification as a BCS superconductor. The band structure analysis reveals the presence of Dirac-like band crossing points, van Hove singularities, and a flat band. The confirmation of the topological non-trivial electronic structures of 1T-RhSeTe is achieved through the evolution of WCCs and time-reversal symmetry-protected topological surface states (TSSs). The coexistence of superconductivity and topological electronic states in 1T-RhSeTe indicates that it may be a promising candidate for topological superconductivity.

## Acknowledgments

Project supported by the National Natural Science Foundation of China (Grant No. 12204400), Science Research Project of Hebei Education Department (Grant No. QN2022169), the Natural Science Foundation of Hebei Province (Grant Nos. A2022203010 and A2024203011), and Innovation Capability Improvement Project of Hebei Province (Grant No. 22567605H).

## References

[1] Di Sante D, Das P K, Bigi C, Ergönenc Z, Gürtler N, Krieger J A, Schmitt T, Ali M N, Rossi G, Thomale R, Franchini C, Picozzi S, Fujii J, Strocov V N, Sangiovanni G, Vobornik I, Cava R J and Panaccione G 2017 *Phys. Rev. Lett.* **119** 026403

[2] Wu S, Fatemi V, Gibson Q D, Watanabe K, Taniguchi T, Cava R J and Jarillo-Herrero P 2018 *Science* **359** 76

[3] Costanzo D, Jo S, Berger H and Morpurgo A F 2016 *Nat. Nanotechnol.* **11** 339

[4] Fang Y, Pan J, He J, Luo R, Wang D, Che X, Bu K, Zhao W, Liu P, Mu G, Zhang H, Lin T and Huang F 2018 *Angewandte Chemie International Edition* **57** 1232

[5] Bruyer E, Di Sante D, Barone P, Stroppa A, Whangbo M H and Picozzi S 2016 *Phys. Rev. B* **94** 195402

[6] Strachan J, Masters A F and Maschmeyer T 2021 *ACS Applied Energy Materials* **4** 7405

[7] Lian C S, Si C and Duan W 2020 *Nano Lett.* **21** 709

[8] He W Y, Zhou B T, He J J, Yuan N F Q, Zhang T and Law K T 2018 *Commun. Phys.* **1** 1

[9] Zhao C X, Liu J N, Li B Q, Ren D, Chen X, Yu J and Zhang Q 2020 *Adv. Funct. Mater.* **30** 2003619

[10] Kusmartseva A F, Sipos B, Berger H, Forro L and Tutis E 2009 *Phys. Rev. Lett.* **103** 236401

[11] Xiao R C, Gong P L, Wu Q S, Lu W J, Wei M J, Li J Y, Lv H Y, Luo X, Tong P, Zhu X B and Sun Y P 2017 *Phys. Rev. B* **96** 075101

[12] He Q L, Liu H, He M, Lai Y H, He H, Wang G, Law K T, Lortz R, Wang J and Sou I K 2014 *Nat. Commun.* **5** 4247

[13] Ermolaev G, Voronin K, Baranov D G, Kravets V, Tselikov G, Stebunov Y, Yakubovsky D, Novikov S, Vyshnevyy A, Mazitov A, Kruglov I, Zhukov S, Romanov R, Markeev A M, Arsenin A, Novoselov K S, Grigorenko A N and Volkov V 2022 *Nat. Commun.* **13** 2049

[14] Yan M, Huang H, Zhang K, Wang E, Yao W, Deng K, Wan G, Zhang H, Arita M, Yang H, Sun Z, Yao H, Wu Y, Fan S, Duan W and Zhou S 2017 *Nat. Commun.* **8** 257

[15] Tanisha T T, Hossain M S, Hiramony N T, Rasul A, Hasan M Z and Khosru Q D M 2024 arXiv:2401.13124 [cond-mat.mtrl-sci]

[16] Sato M and Ando Y 2017 *Reports on Progress in Physics* **80** 076501

[17] Gu K Y, Luo T C, Ge J and Wang J 2020 *Acta Phys. Sin.* **69** 020301 (in Chinese)

[18] Nayak C, Simon S H, Stern A, Freedman M and Das Sarma S 2008 *Rev. Mod. Phys.* **80** 1083

[19] Sarma S D, Freedman M and Nayak C 2015 *npj Quantum Information* **1** 1

[20] Liu C C, Lu C, Zhang L D, Wu X, Fang C and Yang F 2020 *Phys. Rev. Res.* **2** 033050

[21] Fidkowski L 2010 *Phys. Rev. Lett.* **104** 130502

[22] Qi X L and Zhang S C 2011 *Rev. Mod. Phys.* **83** 1057

[23] Patra C, Agarwal T, Arushi, Manna P, Bhatt N, Singh R S and Singh R P 2023 arXiv:2311.01019 [cond-mat.supr-con]

[24] Geller S 1955 *J. Am. Chem. Soc.* **77** 2641

[25] Lurgo F E, Pomiro F, Carbonio R E and Sanchez R D 2022 *Phys. Rev. B* **105** 104104

[26] Kresse G and Hafner J 1993 *Phys. Rev. B* **47** 558

[27] Perdew J P, Burke K and Ernzerhof M 1996 *Phys. Rev. Lett.* **77** 3865

[28] Kresse G and Joubert D 1999 *Phys. Rev. B* **59** 1758

[29] Klimeš J, Bowler D R and Michaelides A 2009 *J. Phys.: Condens. Matter* **22** 022201

[30] Giannozzi P, Andreussi O, Brumme T, *et al.* 2017 *J. Phys.: Condens. Matter* **29** 465901

[31] Mostofi A A, Yates J R, Pizzi G, Lee Y S, Souza I, Vanderbilt D and Marzari N 2014 *Computer Physics Communications* **185** 2309

[32] Mostofi A A, Yates J R, Lee Y S, Souza I, Vanderbilt D and Marzari N 2008 *Computer Physics Communications* **178** 685

[33] Poncé S, Margine E R, Verdi C and Giustino F 2016 *Computer Physics Communications* **209** 116

[34] Allen P B 1972 *Phys. Rev. B* **6** 2577

[35] Allen P B and Dynes R C 1975 *Phys. Rev. B* **12** 905

[36] Wu Q, Zhang S, Song H F, Troyer M and Soluyanov A A 2018 *Computer Physics Communications* **224** 405

[37] Yu R, Qi X L, Bernevig A, Fang Z and Dai X 2011 *Phys. Rev. B* **84** 075119

[38] Kane C L and Mele E J 2005 *Phys. Rev. Lett.* **95** 146802

[39] Soluyanov A A and Vanderbilt D 2011 *Phys. Rev. B* **83** 035108

[40] Chen W, Shen T, Feng Y, Liu C, Liu X and Wu Y 2023 *Physica Scripta* **98** 105531

[41] Akiba K and Kobayashi T C 2023 *Phys. Rev. B* **107** 245117

[42] Fu L and Kane C L 2008 *Phys. Rev. Lett.* **100** 096407

[43] Li X D, Yu Z D, Chen W P and Gong C D 2022 *Chin. Phys. B* **31** 110304

[44] Zhu Z L, Liu Z L, Wu X, Li X Y, Shi J A, Liu C, Qian G J, Zheng Q, Huang L, Lin X, Wang J O, Chen H, Zhou W, Sun J T, Wang Y L and Gao H J 2022 *Chin. Phys. B* **31** 077101

[45] Wang Z, Dong H, Zhou W, Cheng Z and Wang S 2023 *Chin. Phys. B* **32** 067103